DE GRUYTER OPEN

10.1515/mecdc-2018-0004

PHYSICAL 1D MODEL OF A HIGH-PRESSURE RATIO CENTRIFUGAL COMPRESSOR FOR TURBOCHARGERS

JAN MACEK
Czech Technical University in Prague, Center of Vehicles for Sustainable Mobility, Technická 4, 166 07 Praha 6, Czech Republic
Email: jan.macek@fs.cvut.cz

ABSTRACT

The physical model of a centrifugal compressor aims at finding detailed information on values inside the machine, based on standard compressor map knowledge and basic geometry of a compressor. The model describes aerodynamics of flow from compressor inlet to outlet at a central streamline, if mass flow rate and impeller speed is known. The solution of basic conservation laws can yield unknown, cross-section averaged temperatures, pressures and velocities along central streamline for compressible fluid and treats transonic operation, as well. After the description of general methods for solving compressible fluid flow and transformation of radial blade cascades to axial ones, the system of equations is completed with empiric knowledge of compressor blade cascades – forces and losses. Howell theory is used for axial inducer and after conform transformation to radial blade diffuser cascade, as well. Radial vanes of a rotor are transformed fixing the same length of a blade and flow areas and flow separation at inducer outlet is taken into account. Specific procedure is developed for a vaneless diffuser with friction losses. Non-linear equations of gas dynamics have to be solved in numerical and iterative way with help of Newton-Raphson solver. The model treats transonic flow features in both compressor inducer and diffuser. The validation of the model will be published in the second paper focused to this topic.

The model can be used for quasi-steady simulation in a 1D model, especially if compressor map extrapolation is required. The model predictions create virtual sensors for identification of directly unmeasurable quantities inside a compressor. It helps in better understanding in-compressor processes. Moreover, the model offers parameters for unsteady model, based on 1D modules for unsteady flow modelling.

KEYWORDS: CENTRIFUGAL COMPRESSOR, 1D SIMULATION, PHYSICAL MODEL OF COMPRESSOR MAP, TRANSONIC PERFORMANCE, RADIAL DIFFUSER

SHRNUTÍ

Fyzikální model odstředivého kompresoru je zaměřen na odhad stavů proudu uvnitř kompresoru na základě změřené charakteristiky a základních geometrických rozměrů stroje. Model popisuje aerodynamiku proudu na střední proudnici od vstupu do záběrníku po výstup ze spirály pro známý hmotnostní průtok a otáčky rotoru. Řešení základních zákonů zachování určuje neznámé střední teploty, tlaky a rychlosti podél střední proudnice pro stlačitelnou tekutinu a bere v úvahu i transsonické stavy proudu. V článku jsou popsány použité iterační metody řešení proudění stlačitelné tekutiny v radiálních mřížích s využitím jejich konformního zobrazení na axiální mříž. Soustava základních rovnic pak může být doplněna o empirické poznatky o silách a ztrátách v axiálních mřížích, zejména pomocí Howellovy teorie pro záběrník rotoru a po konformní transformaci i pro radiální mříž difusoru. Radiální lopatky oběžného kola jsou transformovány na ekvivalentní difusor se stejnou délkou a poměrem průřezů, i s ohledem na separační bublinu na výstupu ze záběrníku. Nová metoda je vyvinuta pro modelování bezlopatkového difusoru s třecími ztrátami. Nelineární soustava rovnic dynamiky plynů je řešena iteracemi s použitím Newton-Raphsonovy metody. Model bere v úvahu transsonické poměry na vstupu do záběrníku a do bezlopatkového difusoru. Validace modelu bude předmětem dalšího článku.

Model lze použít pro kvazi-stacionární simulace kompresoru v 1D modelech motoru, zejména při nutnosti extrapolovat charakteristiku kompresoru. Model vytváří virtuální senzory pro odhad stavů uvnitř kompresoru, které nejsou přímo měřitelné. Pomáhá v pochopení vlivu dějů v kompresoru na jeho vlastnosti. Model nabízí do budoucna i rozšíření při použití modulů s nestacionárním jednorozměrným průtokem pro modelování jednotlivých částí kompresoru.

KLÍČOVÁ SLOVA: ODSTŘEDIVÝ KOMPRESOR, 1D SIMULACE, FYZIKÁLNÍ MODEL CHARAKTERISTIKY KOMPRESORU, TRANSSONICKÝ REŽIM, RADIÁLNÍ DIFUZOR

1. INTRODUCTION AND MOTIVATION

The high-pressure ratios of turbocharger compressors, needed for the current brake mean effective pressure levels, call for the better description and understanding of processes inside centrifugal compressors. Even using 1D approach only, suitable for repeated optimization simulations, the model can yield interesting results, if it is based on physical description of processes.

The paper aims at the 1D, quasi-steady, central streamline model of a centrifugal compressor with axial-radial flow, suitable for 1D engine models with unsteady conditions during the both transient load and speed of a car engine – general requirements being described already in [12] and [13]. The developed model of a centrifugal compressor describes the aerodynamics of flow from compressor inlet if mass flow rate and impeller speed is known. The basic idea of solution of basic conservation laws has been successfully tested for the case of centripetal radial-axial turbine – [1] and [2]. There are already such models, e.g., [15] or [16]. The current model tries to treat better transonic phenomena and use the available knowledge from axial compressor cascades taking the real asymmetric incidence angle influence into account, better than old NACA shock loss theory [4] for today's shapes of inlet blade profile.

The main goal is a development of the compressor physical model for compressible fluid flow at the reasonable level of simplification for compressor performance description. The developed model will be validated by fitting to known compressor maps aiming at extrapolation of maps and better prediction of surge and choke lines.

The model validation testing will be done against measured maps. Finding fitting (correction) coefficients by optimization methods is realized in a similar way, as it was done for the case of radial centripetal turbine, e.g. [1].

The solution of basic conservation laws can yield unknown temperatures, pressures and velocities along central streamline for compressible fluid and treats transonic operation, as well. After the description of general methods for solving compressible fluid flow and transformation of radial blade cascades to axial ones as done partially in [3], the system of equations is completed with empiric knowledge of compressor blade cascades losses. Howell theory – [4] and [5], originally published in [7] and [8] is used for axial inducer and after transformation fixing the same length of a blade and flow areas to radial blade cascades, as well.

Non-linear equations of gas dynamics have to be solved in numerical and iterative way with help of Newton solver. The treatment of transonic flow features in both compressor inducer and diffuser is described then, based on gas dynamics as described in [14]. The general compressor parameters are finally evaluated from detailed cascade description, making advantage from the modular design of the model.

The model yields information, which could be received from virtual sensors of values inside a compressor. It is suitable for the assessment of collaboration between stages in multi-stage machines and two-stage turbocharging. In the future, the model will be used for the elucidation of compressor design issues and the proposal of ways improving compressor design.

The validation of the model will be published in the second paper focused to this topic.

Moreover, the model offers parameters for unsteady model, based on 1D modules for unsteady flow modelling, as done in [1], [2] or [16].

The paper is structured in the following manner: first, geometry of blades and flow are described, taking the later use of profile cascade theory for lift and drag forces into account. Relations for combination of mass and energy conservation laws are solved for finding procedures to determine total, stagnation and static states for compressible fluid dynamics then. Loss definitions for diffuser and nozzle flows are treated after it in the form of numerical procedures. Generalized results of axial profile blade theory are applied for compressor simulations after it. Specific attention is devoted to a vaneless diffuser with compressible fluid flow. Transonic performance of inducer inlet and vaneless diffuser is analyzed then. Finally, the basic compressor component description and their interaction is described.

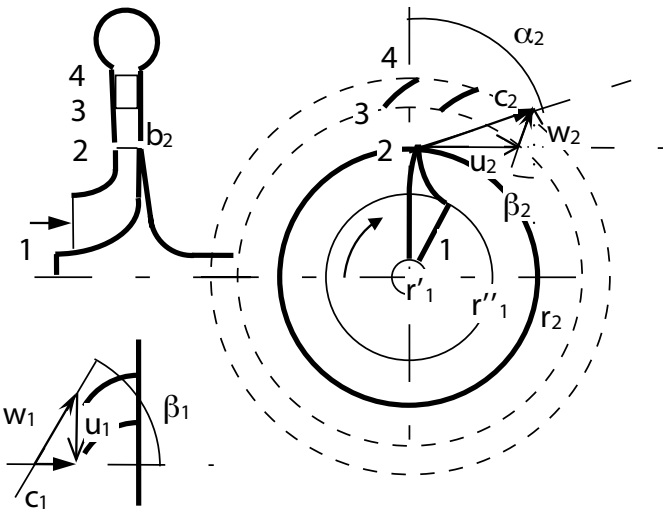

FIGURE 1: A compressor impeller (1-2) and diffuser (2-3 vaneless, 3-4 bladed) with positive sense of flow and blade angles (in reality, outlet from impeller features negative vane angle).

OBRÁZEK 1: Oběžné kolo kompresoru (1-2) a difusor (2-3 bezlopatkový, 3-4 lopatkový) s kladným směrem rychlostí a úhlů lopatek. U skutečných kompresorů je úhel výstupní části lopatek oběžného kola záporný.

2. GEOMETRY OF RADIAL COMPRESSOR FLOW

The compressor performance will be described at fixed mass flow rate and impeller speed with known geometry – at any location defined by the radius r, axial width b, step of blades in cascade s, blade chord c and blade angle measured from radius α_B or β_B for a stator or impeller, respectively. The positive direction of angle is measured in sense of impeller rotation. General scheme of radially-axial centrifugal compressor is plotted in Figure 1.

Defining flow angles by α or β for a stator or impeller, respectively, the velocity triangles and splitting vectors into tangential or axial/radial components yield, e.g.,

$$w_2 \cos\beta_2 = w_{2r} = c_{2r} = c_2 \cos\alpha_2$$
$$\vec{c}_{2t} = u_2 + \vec{w}_{2t} = u_2 + w_{2r} \tan\vec{\beta}_2 \qquad (1)$$

Symbols with arrows respect by their signs the real direction (positive in the direction of rotation), without signs are always positive (absolute values of vectors).

A radial blade cascade may be converted into the axial one using conform (angle conserving) transformation from radial-tangential cylindrical coordinates into Cartesian axial-tangential coordinates, used usually for profile cascade.

The transformation assumes constant density (or density compensated by the appropriate change of axial width b) and angular momentum conservation in a free vortex flow. Then, the both radial and axial components of velocity in polar coordinates are variable, but the product of velocity component and radius is conserved. The transformation is based on the same radial and axial area and rescaling of $d\varphi$ and $d(br)$ by the same constant factor. If channel width b is constant, then the angles of flow are conserved (conform transformation) and, especially, the velocity angle from radial direction is constant.

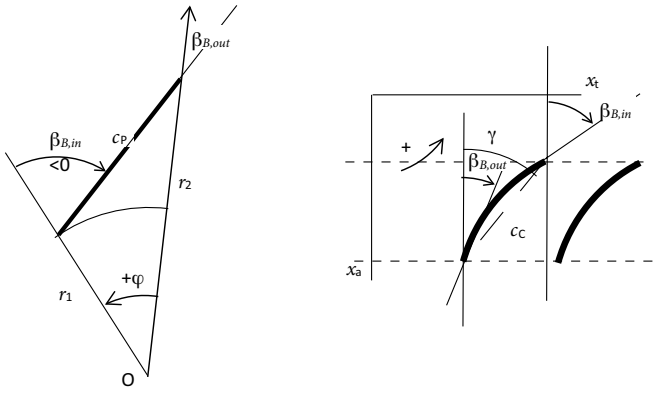

FIGURE 2: Conform transformation of general straight line from polar coordinates.
OBRÁZEK 2: Konformní zobrazení obecně položené přímky z polárních souřadnic.

$$d\phi = \frac{b_{ref} K_2}{br} dx_t \; ; \quad \frac{d(br)}{br} = \frac{b_{ref} K_2}{br} dx_a \qquad (2)$$

$$k_2\left(x_{a,out} - x_{a,in}\right) = k_2 c \cos\gamma = \ln\left(\frac{(br)_{out}}{(br)_{in}}\right)$$
$$\Delta\phi = k_2\left(x_{t,out} - x_{t,in}\right); \quad k_2 = \frac{2\pi}{zs}; \quad z = \frac{2\pi\cos\gamma}{\frac{s}{c}\ln\left(\frac{(br)_{out}}{(br)_{in}}\right)} \qquad (3)$$

For basic directions in axial or tangential straight line in Cartesian coordinates transformation yields for constant blade height radial straight line or the arc of a circle, respectively. General straight lines are transformed into logarithmic spirals. Points of blade surface can be transformed using

$$x_t - x_{t,in} = \frac{c\cos\gamma\left(\phi - \phi_{in}\right)}{\ln\left(\frac{(br)_{out}}{(br)_{in}}\right)}; \quad x_a - x_{a,in} = c\cos\gamma\frac{\ln\frac{r}{r_{in}}}{\ln\left(\frac{(br)_{out}}{(br)_{in}}\right)} \qquad (4)$$

The variability of blade height can be taken into account by this transformation, but the angles of flow are not the same as in Cartesian coordinates more. The influence of centrifugal force from flow curvature and its influence on boundary layer (BL) development cannot be taken fully into account, of course. The same is valid for impeller centrifugal force, if applicable. Although the transformation has to be corrected by calibration coefficients, the qualitative validity of this approach was several times proven for radial turbines, as in [3].

In the case of compressor impeller, the angles from radial direction are small, sometimes even zero (radial vanes), but mostly backswept (Figure 3). Even in the case of radial vanes, the flow inside impeller channels is not equivalent to purely straight diffuser channel. Lift force from flow direction change in an axial cascade is replaced in the case of radial flow by the lift force created by Coriolis inertia force. Instead of centrifugal force due to channel curvature in an axial cascade, Coriolis force acts on the flow, if radial velocity component exists.

Coriolis force causes pressure distribution in tangential direction with increase of pressure in counter-rotation direction (counter-clockwise in Figure 3). This pressure distribution is followed by the flow separation at the suction side of a vane being ahead in the sense of rotation. It is reflected by the outlet velocity profile, called "jet and wake" with flow separation bubble behind the leading vane and with jet part of flow close to the pressure side of the following vane.

The equivalence of the centrifugal force in a curved axial channel and Coriolis force in an impeller channel can be used for the estimate of deviation angle and losses in an impeller. Only one

half of Coriolis acceleration has to be used since the flow features (almost) zero angular speed due to the slip of flow relative to vanes. Using the same flow-bearing velocities for both equivalent cascades in radial (subscript r) and axial direction (a), respectively, the force acting on the element of flow with the mass of Δm is

$$w_r = \frac{\dot{m}}{\left(2\pi r_r - z b_{B,r}\right) b_r \rho} = w_a = \frac{\dot{m}}{\pi\left(r_a''^2 - r_a'^2\right)\rho} = w\cos\beta_{B,a}$$

$$F_{Co} = \Delta m \omega w_r \equiv F_{cent} = \Delta m \frac{w^2}{R} \Rightarrow \frac{\omega}{w_r} = \frac{1}{\cos^2\beta_{B,a}} \frac{y''}{\sqrt{\left(1+y'^2\right)^3}} \quad (5)$$

where y is a axial blade centerline shape, described by function of axial coordinate and derived for finding local curvature. Then, the differential equation for transformed axial blade cascade centerline can be found from its curvature using obvious

$$\frac{1}{\cos^2\beta_{B,a}} = \tan^2\beta_{B,a} + 1 = y'^2 + 1$$
$$y'' = \frac{\omega}{w_r}\sqrt{1+y'^2} \quad (6)$$

which can be integrated for $tan\ \beta_{B,a}$ using Euler's substitution.
The described transformations can help to some extent for the estimation of losses, based on old but yet worthwhile generalizations of axial diffuser blade cascades – e.g., Howell [7], [8] and [5]. Unlike estimation of incidence loss by old shock loss theory, it takes the real behavior of BL into account better. The boundary layer development in an impeller is influenced by relative vortex, moreover (see equation (33)), that is why correction by calibration coefficient is necessary.

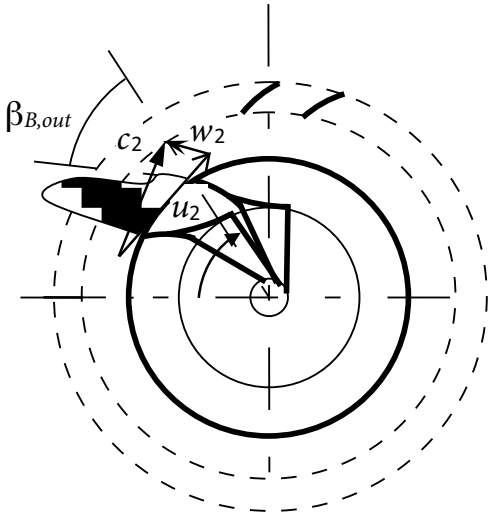

FIGURE 3: Backswept impeller vans and impeller outlet velocity profile (jet and wake).
OBRÁZEK 3: Oběžné kolo s dozadu zahnutými lopatkami. Rychlostní pole na výstupu z kanálu dle teorie proudu na přetlakové straně lopatky a úplavu na podtlakové straně.

3. TOTAL, STAGNATION AND STATIC STATES

Stodola equation for energy conservation yields, using velocities c in steady (absolute) coordinate system or w in relative (rotating) coordinate system with relative or absolute stagnation (0) states and total state (t):

$$dh + d\frac{c^2}{2} = dh_0 = 0$$
$$dh + d\frac{w^2}{2} - d\frac{u^2}{2} = dh_{0,rel} - d\frac{u^2}{2} = dh_t = 0 \quad (7)$$

E.g., for a rotating impeller it yields after integration

$$c_p T_{0,rel,out} = c_p T_{out} + \frac{w_{out}^2}{2} = c_p T_{0,rel,in} + \frac{u_{out}^2 - u_{in}^2}{2} \quad (8)$$

Non-linear equations of gas dynamics have to be solved in numerical and iterative way with help of Newton solver, as follows. If static state and mass flow rate are known, finding total state is without any numerical problem. The velocity of flow can be found from static density for reversed relation. Total temperature is

$$T_t = T + \frac{w^2}{2c_p} - \frac{u^2}{2c_p} \quad (9)$$

Total or stagnation pressure is defined by isentropic change. In the case of stagnation pressure, it yields

$$p_0 = p\left(\frac{T_0}{T}\right)^{\frac{\kappa}{\kappa-1}} \quad (10)$$

The most complicated case often occurs in a compressor description. The system of equations (9) and (10) can be replaced together with mass flow rate equation by

$$T_0 = T + \frac{1}{2c_p}\left(\frac{\dot{m}}{A\rho_0}\right)^2 \left(\frac{T_0}{T}\right)^{\frac{2}{\kappa-1}} \quad (11)$$

and solved using Newton's method for unknown static temperature

$$y = T_0 - T - \frac{1}{2c_p}\left(\frac{\dot{m}}{A\rho_0}\right)^2 \left(\frac{T_0}{T}\right)^{\frac{2}{\kappa-1}} \approx y_i + \left(\frac{dy}{dT}\right)_i \left(T_{i+1} - T\right) should\ be\ 0$$

$$\frac{dy}{dT} = -1 + \frac{1}{c_p(\kappa-1)}\left(\frac{\dot{m}}{A\rho_0}\right)^2 T_0^{\frac{2}{\kappa-1}} T^{-\frac{\kappa+1}{\kappa-1}} = -1 + \frac{1}{\kappa r}\left(\frac{\dot{m}}{A\rho_0}\right)^2 T_0^{\frac{2}{\kappa-1}} T^{-\frac{\kappa+1}{\kappa-1}}$$

$$0 = y_i + \left(\frac{dy}{dT}\right)_i \left(T_{i+1} - T_i\right) \Rightarrow T_{i+1} = T_i - \frac{y_i}{\left(\frac{dy}{dT}\right)_i} \quad (12)$$

Derivative of function in denominator must not be zero, which yields temperature limit. This temperature is just a critical temperature. If iteration result is limited to temperature greater

than this limit (and less than T_0), it yields subsonic solutions. It can be used for supersonic case, as well, if started with temperature less than limit one.

In the case of rotating channel, the similar procedure can be found. If critical state is reached, energy conservation yields between inlet and outlet

$$T^*_{out} = \frac{1}{\kappa r}\left[\kappa r T_{0in}\frac{2}{\kappa+1} + \frac{\kappa+1}{\kappa-1}\left(u^2_{out} - u^2_{in}\right)\right] \tag{13}$$

If the equation (13) is applied to calculation of static temperature from total one, the influence of centrifugal force energy is zero. The relation is valid for any adiabatic case including irreversibility. If supersonic inlet occurs, the result has to be carefully assessed from the point of view of physical stability of such solution. E.g., in the case of inducer inlet, the solution for too high mass flow rate, which would lead to further acceleration of supersonic flow in the following diffuser blade cascade, is not probably real. The inducer is choked at inlet by shock wave perpendicular to flow direction in such a case and the assumed mass flow rate cannot be reached. The maximum mass flow rate has to be calculated in advance for the static temperature from equation (13). In 3D reality, the process of choking is much more complicated and increases incidence loss via the series of oblique shocks in blade channel inlet, but the choking mass flow rate is valid, if the inlet area is corrected to possible boundary layer separation caused by λ-like shocks in boundary layer. The situation is more complicated if transonic flow velocity is caused by high speed of impeller. Further examples follow below.

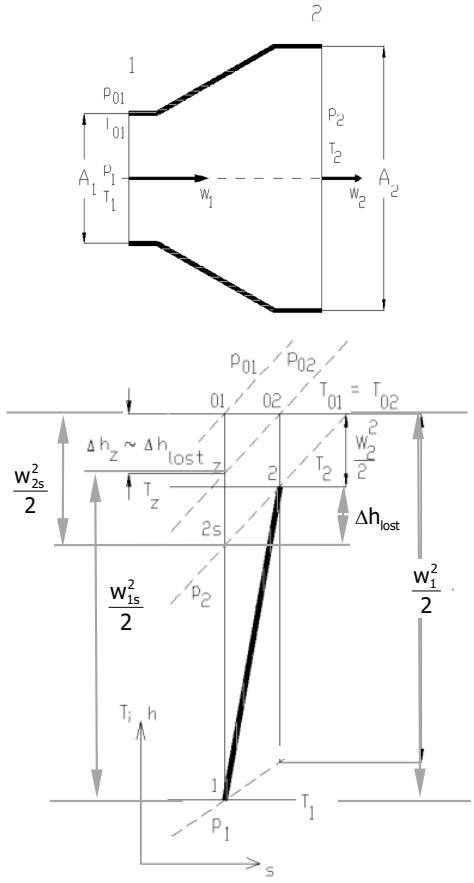

FIGURE 4: Diffuser flow and definition of losses in T-s diagram.
OBRÁZEK 4: Proudění difuzorem a definice ztrát v T-s diagramu.

4. DIFFUSER FLOW AND LOSSES

The isentropic efficiency and loss coefficient of diffuser flow is defined according to Figure 4 by the following relations

$$\eta_{in} = \frac{\frac{w^2_{1s}}{2}}{\frac{w^2_1}{2}} = 1 - \frac{\Delta h_z}{\frac{w^2_1}{2}} = 1 - \zeta_{in} \tag{14}$$

Should resulting temperature or density be determined, the procedure described above has to be changed, taking losses of kinetic energy and potential energy centrifugal force field into account. Then, it yields for compressor flow through a generally rotating diffuser cascade with known state at blade inlet *in* the static state at outlet *out* the basic relation for Newtonian iteration, similar to

$$y = T_{0in} - \frac{u^2_{in} - u^2_{out}}{2c_p} - T_{out} - \frac{1}{2c_p}\left(\frac{\dot{m}}{A\rho_{0in}}\right)^2 \left(\frac{\frac{T_{out}}{T_{0in}}}{\left[\frac{T_{out}}{T_{0in}} - \zeta_{in}\left(1 - \frac{T_{in}}{T_{0in}}\right)\right]^{\frac{\kappa}{\kappa-1}}}\right)^2 \tag{15}$$

The derivative of y can be easily found in analytical way and applied to (12). The temperature has to be greater than critical one according to (13) for subsonic solution.

5. GENERALIZATION OF AXIAL BLADE CASCADE RESULTS

5.1 GEOMETRY OF AXIAL PROFILE CASCADE

The angles of flow are measured from axial direction. The blade angles are β_B, the angles of flow in coordinate system of blade cascade (relative flow coordinates) are β, the angles of flow in steady (absolute) coordinate system are α. The following relations are used for flow turn angle, incidence angle and outlet deviation angle

$$|\varepsilon| = |\beta_{in}| - |\beta_{out}|$$
$$|\iota| = |\beta_{in}| - |\beta_{B,in}| \tag{16}$$
$$|\delta| = |\beta_{B,out}| - |\beta_{out}|$$

Moreover, the airfoils are described by length of chord c, cascade step s, maximum distance of airfoil centerline from chord p angles of tangent to centerline measured from axial direction β_B.

5.2 HOWELL THEORY OF COMPRESSOR BLADE CASCADES

The losses have to be added from profile loss of planar airfoil cascade (surface friction and wake losses), secondary losses caused by induced vortices and blade tip losses.

Profile loss coefficient is calculated from drag coefficient at central streamline, using mean diameter of axial blades (if relevant) and blade step

$$R_{mean} = \sqrt{\frac{R''^2 + R'^2}{2}}; \quad s = \frac{2\pi R_{mean}}{z} \tag{17}$$

Profile cascade features can be found using Howell's approach generalizing angle of flow turn and drag coefficient for profile cascades.

The normalized angle of flow turn $\varepsilon / \varepsilon^*$ can be found from the empirical dependence of normalized angle of incidence $(\iota - \iota^*)/\varepsilon^*$ in Figure 5. Drag coefficient c_x depends on normalized step of cascade. All curves can be substituted by polynomial regressions. In the case of flow turn angle, it is amended additionally by exponential correction to separation of boundary layer

$$\frac{\varepsilon}{\varepsilon^*} = \left(a_0 + \sum_1^6 a_i \left(\frac{\iota - \iota^*}{\varepsilon^*} \right)^i + a_{13} \left(\frac{\iota - \iota^*}{\varepsilon^*} \right)^{13} \right) \left(1 - e^{\left(\frac{\frac{\iota - \iota^*}{\varepsilon^*} - 0.95}{0.4} \right)^7} \right) \tag{18}$$

Reference values can be found from reference deviation angle (Constant's rule, NACA – [4])

$$|\beta_{out}^*| = |\beta_{B,out}| + \delta^*; \quad \delta^* = \frac{0.23\left(\frac{2p}{c}\right)^2 + \frac{|\beta_{B,out}|}{500}}{\frac{1}{|\theta|\sqrt{\frac{s}{c}}} - \frac{1}{500}}; \tag{19}$$
$$|\theta| = |\beta_{B,in}| - |\beta_{B,out}|$$

and Howell's relation

$$\tan|\beta_{in}^*| - \tan|\beta_{out}^*| = \frac{1.55}{1 + 1.5\frac{s}{c}} = S \tag{20}$$

Angles are bound by the following relations

$$\varepsilon^* = |\beta_{in}^*| - |\beta_{out}^*|; \quad |i^*| = \varepsilon^* - |\theta| + \delta^* \tag{21}$$

which yields for reference flow turn angle a quadratic equation from (20) and (21) with the solution

$$|\varepsilon^*| = \arctan \frac{-\frac{1}{(\cos\beta_{out}^*)^2} + S\tan|\beta_{out}^*| + \sqrt{\left(\frac{1}{(\cos\beta_{out}^*)^2} - S\tan|\beta_{out}^*|\right)^2 + 8S\tan|\beta_{out}^*|}}{4\tan|\beta_{out}^*|} \tag{22}$$

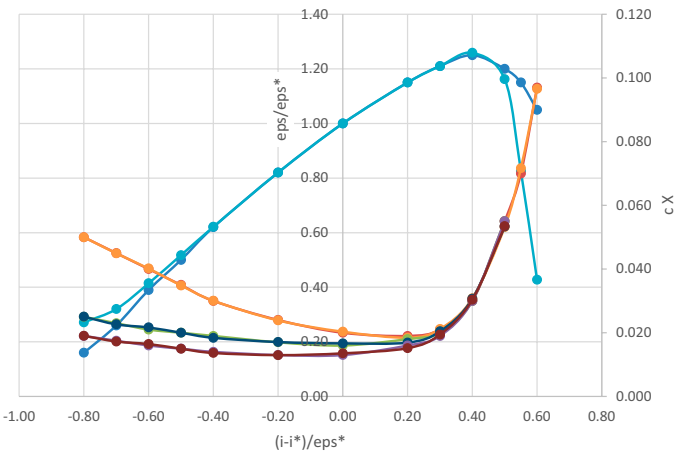

FIGURE 5: Relative angle of flow turn *eps* normalized by reference angle *eps** and profile drag coefficient *c X* for compressor blade cascade – [7]. Drag coefficient for different relative steps s/c 0.5, 1. and 1.5, as mentioned in curve descriptions. Dependences on the difference of angle of incidence ι and its reference value ι^* normalized by reference flow turn angle *eps**. Comparison of published data and regression model.

OBRÁZEK 5: Poměrný úhel natočení proudu *eps* normovaný jmenovitým úhlem *eps** a profilový součinitel odporu *c X* pro kompresorovou profilovou mříž – [7]. Součinitel odporu pro různé poměrné rozteče s/c 0.5, 1. a 1.5. Závislosti na poměrné odchylce úhlu náběhu ι od jmenovitého úhlu ι^*. Srovnání publikovaných dat a regresního modelu.

Reference values are calculated once for the whole compressor map prediction. Radial cascades in a vaned diffuser are transformed to axial ones using (4).
Then using (18)

$$\vec{\iota} = |\beta_{in}| - |\beta_{B,in}|; \quad |\varepsilon| = \varepsilon^* \left(\frac{\varepsilon}{\varepsilon^*} \right) = f\left(\varepsilon^*, \iota^*, \iota\right); \tag{23}$$

$$\vec{\beta}_{out} = |\beta_{in}| - |\varepsilon|$$

and drag coefficient can be found. Incidence angle influence is described in a better way than by NACA shock loss theory referred to in [15].

5.3 FORCES IN A BLADE CASCADE

Tangential T and axial A forces in an axial compressor blade cascade, acting from fluid to airfoils can be found from lift and drag forces using mean angle of flow – [4] – with positive directions defined in Figure 2 and for the case of compressor

$$\vec{T} = \text{sign}\left(\vec{\beta}_m\right) F_y \cos\beta_m + F_x \sin\vec{\beta}_m; |T| = F_y \cos\beta_m + F_x \sin|\beta_m|$$

$$\vec{A} = -F_y \sin|\vec{\beta}_m| + F_x \cos\beta_m; |A| = F_y \sin|\vec{\beta}_m| - F_x \cos\beta_m \tag{24}$$

using

$$\vec{\beta}_m = \arctan\left(\frac{\tan\vec{\beta}_{in} + \tan\vec{\beta}_{out}}{2} \right) \tag{25}$$

and well-known definition with lift and drag coefficients, replacing velocity in infinity by its axial component and mean angle of flow

$$F_y = c_y c \frac{\overline{\rho b}}{2} \frac{w_a^2}{\cos^2\beta_m}; \quad F_x = c_x c \frac{\overline{\rho b}}{2} \frac{w_a^2}{\cos^2\beta_m} \tag{26}$$

Drag force acts on fluid against mean velocity, lift force is perpendicular to it according to the sign of velocity circulation. If results of momentum conservation are combined with energy conservation, tangential and axial forces are determined

$$\vec{T} = \overline{\rho b}\, s w_a^2 \left(\tan\vec{\beta}_{in} - \tan\vec{\beta}_{out} \right); \quad \vec{\beta}_{out} = \vec{\beta}_{in} - \varepsilon \tag{27}$$

$$\vec{A} = -F_Y \sin|\vec{\beta}_m| + F_X \cos\beta_m = \tag{28}$$

$$= \frac{s\,\overline{b\rho}}{2} w_a^2 \left[-\frac{1-\zeta_{in}}{\cos^2\beta_{in}} + \frac{1}{\cos^2\beta_{out}} \right]$$

The procedure is prepared for Howell cascade results, in which flow angle change ε and drag coefficient c_x are generalized from experiments. Combining relations above, it yields for loss coefficient

$$\zeta_{in,p} = 1 - \tan\vec{\beta}_m \cos^2\beta_{in} \left[2\tan\vec{\beta}_{in} - 2\tan\left(\vec{\beta}_{in} - \varepsilon\right) - \right. \tag{29}$$

$$\left. - \frac{c}{s} \frac{c_X}{\cos\alpha_m} \tan\vec{\beta}_m \right] + \frac{c}{s} \frac{c_X \cos^2\beta_{in}}{\cos\beta_m} - \frac{\cos^2\beta_{in}}{\cos^2\beta_{out}}$$

and lift coefficient can be found from

$$c_y = \frac{2\cos\beta_m}{\text{sign}\vec{\beta}_m} \frac{s}{c} \left(\tan\vec{\beta}_{in} - \tan\left(\vec{\beta}_{in} - \varepsilon\right) \right) - c_X \tan|\beta_m| \tag{30}$$

6. APPLICATION OF PROFILE BLADE CASCADE THEORY TO COMPRESSOR COMPONENTS

Outlet angle from an inducer axial blade cascade can be used for estimation of local flow separation at the start of radial impeller part, using empirical chord length of separated bubble with additional calibration coefficient

$$\Delta s = K_{sep} \left(\sin|\vec{\beta}_{out}| - \sin|\vec{\beta}_{B,out}| \right) \tag{31}$$

The part of cascade step blocked by boundary layer separation is used as contraction coefficient in radial velocity component determination

$$w_r = \frac{\dot{m}}{\left[2\pi R - z\left(t_B + \Delta s\right) \right] b\rho} \tag{32}$$

Outlet angle from impeller (often backswept) vanes has to be corrected to relative vortex in intervane channel, namely subtracting tangential relative velocity component – e.g., in [4] – with correction coefficient, which respects the inter-vane channel area reduction due to vane wall thickness

$$\Delta w_t = -K_S \frac{2\pi R_{2out}}{2 z_{2out}} \cos\beta_{B2out} \omega_I = -K_S \frac{\pi u_{2out}}{z_{2out}} \cos\beta_{B2out} \tag{33}$$

Incidence angle has to be calculated according to upstream flow direction, e.g., from velocity triangles,

$$u + \vec{w}_t = \vec{c}_t; \quad w_a = c_a; \quad \tan\vec{\alpha} = \frac{\vec{c}_t}{w_a}; \quad \tan\vec{\beta} = \frac{\vec{w}_t}{w_a} \tag{34}$$

which yields, e.g., for inducer inlet or impeller outlet

$$\vec{\iota}_{1in} = \arctan\frac{\vec{c}_{1t,in} - u_1}{w_a} - \beta_{B1,in}$$

$$\alpha_{2,out} = \arctan\frac{u_2 - K_S \frac{\pi u_{2out}}{z_{2out}} \cos\beta_{B2out} + w_r \tan\vec{\beta}_{B2,out}}{w_r} \tag{35}$$

with flow rate velocities

$$w_a = \frac{\dot{m}}{K_{sep,a}\left[\pi\left(R''^2 - R'^2\right) - zt_B\left(R'' - R'\right)\right]\rho};$$
$$w_r = \frac{\dot{m}}{K_{sep,r}\left(2\pi R - z\left(t_B + \Delta s\right)\right)b\rho} \tag{36}$$

The profile drag coefficient is found from regression described together with equation (18) and recalculated to loss coefficient according to (29).

Secondary losses depend on lift coefficient square, using classic Glauert results. Secondary loss coefficient has to be added to the profile loss one – see [4], [9] and [6] – for blade length b and radial shroud clearance k including tip losses according to [9]

$$\zeta_{in,s} = \left[\frac{0.04}{\frac{b}{c}} + \frac{0.025\frac{k}{b}}{\frac{s}{c}\cos\beta_{out}}\right]\frac{c_Y^2}{\frac{s}{c}}\frac{\cos^2\beta_{in}}{\cos^3\beta_m} \tag{37}$$

If $Re_{c,w\ in}$<200 000 (it may occur at high-pressure compressor stages stages), correction to Re should be done before loss coefficients are summarized – [4]

$$\frac{\zeta_{2p} + \zeta_{2s}}{\left(\zeta_{2p} + \zeta_{2s}\right)_{Re=2.10^5}} = \left(\frac{2.10^5}{Re_{c,w_2}}\right)^{0.2} \tag{38}$$

otherwise no correction is applied. Then

$$\zeta_{in} = \zeta_{in,p} + \zeta_{in,s} + \zeta_{in,l} \tag{39}$$

All estimations have to be corrected by mentioned calibration coefficients.

6.1 IMPELLER INDUCER

The relations for flow turn angle and loss coefficient can be directly applied to quasi-axial inducer blades with correction coefficients taking into account the influence of Stodola vortex and centrifugal force stabilization of BL in radial part of blades.

6.2 BLADED DIFFUSER

Howell theory [7] or [8] can be used after transformation from polar coordinates to Cartesian ones. The procedure is described by Eqs. (4) and (18) – (24).

6.3 VANELESS DIFFUSER

The classic vaneless diffuser theory assumes free vortex (i.e., angular momentum conservation) for tangential velocity component and mass conservation with constant density for radial velocity component. If constant axial width b of vaneless diffuser (as plotted between positions 2 and 3 in Figure 1) is assumed, well-known logarithmic spiral streamline is achieved. Both assumptions are too much idealized, since recent compressors achieve transonic flow at an impeller outlet, the compressibility of fluid and friction loss at side walls of a vaneless diffuser should be taken into account. Velocity components in absolute space of inlet to a vaneless diffuser are

$$c_{2t,in} = u_2 - K_S\frac{\pi u_{2out}}{z_{2out}}\cos\beta_{B2out} + w_{2r}\tan\beta_{B2out}$$
$$c_{2r,in} = \frac{\dot{m}}{K_{sep,r}2\pi R_{2,in}b_{2,in}\rho_{2,out}} \tag{40}$$

Angular momentum conservation yields for radius greater than the inlet radius of a vaneless diffuser, if turbulent friction at side walls is assumed

$$c_t r = \left(c_t + \frac{dc_t}{dr}dr\right)\left(r + dr\right) + \frac{dM_f}{\dot{m}}$$
$$\frac{dM_f}{\dot{m}} \approx \frac{\frac{K_f}{Re_{2b,c}^{0.2}}\frac{2\pi}{2b}\frac{\bar{\rho}\left(c_{2t,in}^2 + c_{2r,in}^2\right)R_2^2}{2}}{\dot{m}}dr \tag{41}$$
$$c_t = \frac{R_2 c_{2t,in}}{r} + \frac{\frac{K_f}{Re_{2b,c}^{0.2}}\frac{\pi}{b}\frac{\bar{\rho}\left(c_{2t,in}^2 + c_{2r,in}^2\right)R_2^2}{2}}{\dot{m}}\left(\frac{R_2}{r} - 1\right)$$

A simplified assumption has been used for friction torque estimate, considering constant channel with b, angular momentum and mean constant density.

Centrifugal force, inertia force from change of radial velocity and pressure equilibrium yield in cylindrical coordinates

$$\frac{dp}{dr} = \frac{c_t^2}{r}\rho + \frac{dc_r}{dr}\frac{dr}{dt} = \rho\frac{c_t^2}{r} - \rho c_r\frac{dc_r}{dr} \tag{42}$$

Mass and energy conservations for adiabatic case conservation yield

$$\frac{dc_r}{dr} = -\frac{\dot{m}}{2\pi}\frac{b\rho + r\rho\frac{db}{dr} + br\frac{d\rho}{dr}}{\left(rb\rho\right)^2};\quad c_p\frac{dT}{dr} = -c_t\frac{dc_t}{dr} - c_r\frac{dc_r}{dr}$$
$$\frac{dc_r}{dr} = -c_r\frac{b\rho + r\rho\frac{db}{dr}}{rb\rho} - \tag{43}$$
$$-c_r\left(\frac{\rho}{p}\frac{c_t^2}{r} - \frac{\rho}{p}c_r\frac{dc_r}{dr} + \frac{1}{c_pT}\left(c_t\frac{dc_t}{dr} + c_r\frac{dc_r}{dr}\right)\right)$$

which can be solved for radial component derivative numerically, if tangential component derivative is expressed by means of

the equation (41). The vaneless diffuser has to be divided into several radial sectors for at least approximate integration of those differential equations. Narrow circular strips should be used for higher Mach numbers. If Mach number less than 0,5, the sensitivity to density change is small.

Resulting radial velocity, pressure, density and tangential velocity at the outlet radius of a vaneless diffuser can be found without major issues, if the inlet flow is subsonic.

7. TRANSONIC PERFORMANCE

The above deduced procedure can be applied for all blade cascades in a compressor if Mach number is less than approximately 0.7. It is fulfilled for impeller except for inducer inlet, especially at high speeds, as mention in comments to the equation (13).

Even before inducer inlet choking is reached, the local relative velocity Mach number, namely the blade tip Mach number, can exceed transonic limit. Combining velocity triangles, continuity equation

$$w_a = \frac{\dot{m}}{K_{sep,a}\left[\pi\left(R''^2 - R'^2\right) - zt_B\left(R'' - R'\right)\right]\rho_{1in}} = \frac{\dot{m}}{k\pi R''^2 \rho_{1in}} = w_{1in}\cos\beta_{1in} \tag{44}$$

$$k = \frac{\left(R''^2 - R'^2\right) - zt_B\left(R'' - R'\right)}{K_{sep,a}R''^2}$$

and energy conservation with definition of stagnation state and Mach number, the following relation can be found for the blade tip Mach number

$$\dot{m} = \frac{k\pi R''^2 \kappa p_{01in} a_{01in}}{u_1''^2} \frac{M_1''^3 \sin^2\beta_{1in}\cos\beta_{1in}}{\left[1 + \frac{\kappa-1}{2}M_1''^2\cos^2\beta_{1in}\right]^{\frac{1}{\kappa-1}+\frac{3}{2}}} \tag{45}$$

This equation can be applied for mean radius and angle of inducer flow to find the approximate limit of inducer choking, as well. According to measurements, the flow separation coefficient should be corrected. The choking limit may be set by a diffuser, as well, as described below. As a difference to inducer choking, the diffuser choking depends more on compressor speed.

In the dependence of mass flow rates for Mach number greater than 1, the loss coefficient of inducer axial blades should be reduced before critical mass flow rate for the whole blade height is reached – [5].

In the case of a vaneless diffuser, the subsonic assumption might not be the case of current high-pressure compressors. The step-by-step integration of density history from equation (43) can be simultaneously used with assessment of transonic flow issues downstream of an impeller.

Inlet flow to a vaneless diffuser is mostly supersonic in high-pressure compressors today. It is caused by the high blade speed of an impeller. The vaneless part is very important to decrease flow velocity in absolute space before the flow enters bladed diffuser, otherwise intensive shock waves with possible BL separation can occur. If shock wave occurs in the vaneless diffuser, it is an oblique shock of angle σ' measured from direction of absolute flow velocity (90° would mean a transversal shock wave). Due to rotational symmetry, the shock wave line must have circular shape and the angle measured from radial direction is $90°- \sigma'$. There are three possible cases for transonic flow then:

- Angle α of flow velocity from radial direction is greater than $90°- \sigma'$ (angle of flow deviation due to oblique shock is $\theta = 0$ in Figure 6 – [14] and [17])

$$\theta = \sigma - \arctan\left[\tan\sigma\frac{2 + (\kappa-1)M_r'^2\sin^2\sigma}{(\kappa+1)M_r'^2\sin^2\sigma}\right] \tag{46}$$

  The normal component of velocity to the possible shock line is subsonic then and no oblique shock may occur. Integration for subsonic radial velocity can be done together with flow deceleration due to tangential component reduction according to angular momentum conservation – equations (41), (42) and (43); this case is often present in today's compressor designs.
- Angle α of flow velocity from radial direction less than $90°- \sigma'$ but greater than $90°- \sigma'$ *for maximum deviation angle* θ (Figure 6). Oblique shock with supersonic radial velocity component occurs for radial Mach number

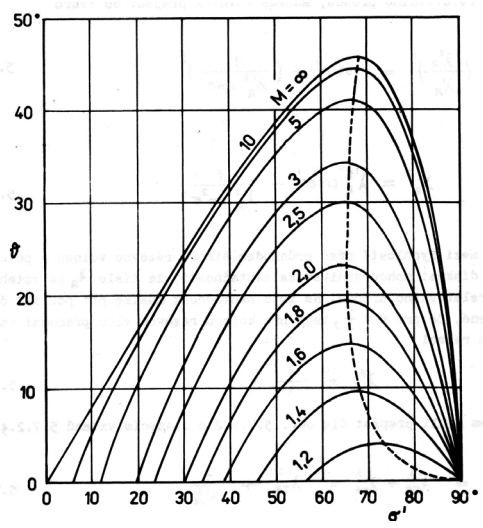

FIGURE 6: Oblique shock: flow deviation angle Θ and shock front angle σ′ measured from velocity direction in front of shock for different initial Mach numbers (from [17]).

OBRÁZEK 6: Šikmá rázová vlna: úhel odklonu proudu Θ a úhle rázové vlny σ′ měřený od směru rychlosti před rázem pro různá počáteční Machova čísla (převzato ze [17]).

$$M_r = \frac{c_r}{a} = \frac{c_r}{\sqrt{\kappa r T}} \tag{47}$$

$$c'_r c''_r = a_r^{*2} = \frac{2}{\kappa+1} a_{0r}^2 = \frac{2\kappa r}{\kappa+1}\left(T + \frac{c_r'^2}{2c_p}\right) \tag{48}$$

$$\frac{\rho''}{\rho'} = \frac{\frac{\kappa+1}{\kappa-1}}{1+\frac{1}{M_r^2}\frac{2}{\kappa-1}}; \quad \frac{p''}{p'} = \frac{2\kappa}{\kappa+1} M_r^2 - \frac{\kappa-1}{\kappa+1} \tag{49}$$

After the shock, subsonic flow equations (41), (42) and (43) can be used.

- Angle α of flow velocity from radial direction is less than *90°- σ' for maximum of θ,* which is approx. 20° (Figure 6). The branches of curves between maximum of flow deviation and lateral shock are unstable. The shock wave tends to be lateral to flow direction, which is impossible due to rotational symmetry in the case of vaneless diffuser. Mass flow rate has to be reduced to achieve the Mach number just for maximum of deviation angle. Choking at a diffuser occurs in this case, which is impeller speed dependent unlike the choking at an inducer according to equation (45) applied to the mean radius of a blade.

8. COMPRESSOR PERFORMANCE

The overall picture of processes inside a compressor is plotted in h-s diagram in Figure 7, using energy conservation for rotating channel, definition of total and stagnation states and velocity triangles.

The simulation procedure is based on known mass flow rate and speed of an impeller. Static states are determined form conservation of total states (Figure 7), mass conservation yielding velocities and loss coefficients, determining entropy increases.

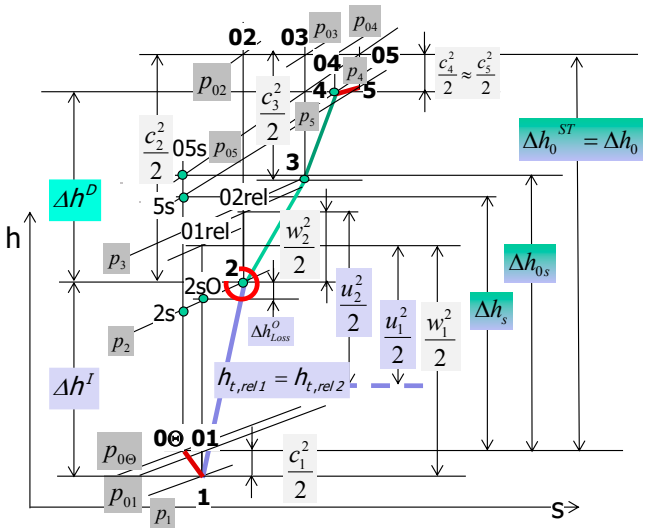

FIGURE 7: h-s diagram of a compressor.
OBRÁZEK 7: h-s diagram kompresoru.

The pressure losses in yet not described parts (an inlet casing or outlet scroll) may be estimated using empirical loss coefficient for friction loss at walls and local losses with approximately constant velocity and density

$$\Delta h_{lost} = \zeta_{out} \frac{w_{out}^2}{2} = \frac{\Delta p_{0,loss}}{\rho_{in}} \tag{50}$$

$$T_{0,in} = T_{0,out}$$

which yields input for the following part of a compressor.

Velocity triangles and decomposition of velocities into axial/radial and tangential components are described by equations similar to (34) for impeller inlet and outlet. Starting with known inlet total state, the static states are determined going from inlet by equations sets (12) and (15).

Flow angles are calculated from Howell theory according to (23) with correction to relative vortex in an impeller – equation (29). Flow area and radial velocity is corrected to local BL separation – equation (31). Loss coefficients are found according to regression similar to (18) after recalculation form drag coefficient to profile loss coefficient (29) adding all partial losses to it in (39).

If inlet and outlet velocities at an impeller are known, the power can be calculated from Eulerian theorem and checked by Stodola for the adiabatic case – see Figure 7

$$P_{C,\text{int}} = \dot{m}\left(c_{t2}u_2 - c_{t1}u_1\right) = \dot{m}c_{pl}\left(h_{02} - h_{0\Theta}\right) \tag{51}$$

Windage loss of an impeller can be estimated from windage power

$$P_{wind} = 0.000735\beta\rho_2 D_2 u_2^3 \dot{m} \tag{52}$$

for β=6 ... 8. Windage power is subtracted from the internal power. Reduced mass flow rate, reduced speed and isentropic efficiency are calculated according to standard definitions.

9. CONCLUSION – PROSPECTS AND FURTHER WORK

The presented physical model of a centrifugal compressor is suitable for compressor simulation in 1D codes if calibrated according to measured compressor maps. On one hand, it uses the basic generalization of experiments valid for axial blade cascades, although amended by certain adoption of radial cascades features, which has to be corrected by available experiments. On the other hand, it treats the transonic flow in the compressors of high-pressure ratio, which yields an opportunity to extrapolate the maps with certain reliability. It is important for choke limit especially. The extrapolation or prediction of surge limits, especially under influence of engine pulsating inlet flow, has not been tested yet. The dynamic surge limit is still certainly a big issue. The procedures for transonic flow prediction are stable and controllable from the

numerical point of view, which ensures reliable behavior during calibration done by optimization.

In any case, the further development and validation of the model is inevitable. The results will be published soon in some of the next MECCA items.

The still remaining items of the further development will cover

- compressor inlet duct loss including the optional use of pre-swirl blades
- leakages at shroud and hub sides influencing back-flow to inducer blades and windage loss at hub side of an impeller
- inducer flow inlet angle corrected to the backflow through a shroud clearance adding angular momentum to inlet flow
- internal recirculation channel (IRC) for surge limit modification
- influence of relative Stodola vortex to secondary vortices in inducer blades (amplification of asymmetry of counter-rotating secondary vortex couple)
- scroll friction and flow separation losses
- the impact of an outlet diffuser located downstream of a scroll
- heat transfer in a compressor casing.

ACKNOWLEDGMENTS

This research has been realized using the support of Technological Agency, Czech Republic, program Centre of Competence, project #TE01020020 Josef Božek Competence Centre for Automotive Industry and The Ministry of Education, Youth and Sports program NPU I (LO), project # LO1311 Development of Vehicle Centre of Sustainable Mobility. This support is gratefully acknowledged.

REFERENCES

[1] Macek, J., Zak, Z., and Vitek, O., Physical Model of a Twin-scroll Turbine with Unsteady Flow, SAE Technical Paper 2015-01-1718, 2015, doi:10.4271/2015-01-1718.

[2] Macek J., Vítek O., Burič J. and Doleček V.: Comparison of Lumped and Unsteady 1-D Models for Simulation of a Radial Turbine. SAE Int. J. Engines Vol.2(1) 173-188, 2009, ISSN 1946-396. SAE Paper 2009-01-0303

[3] Sherstjuk, A. N., Zaryankin, A.E., "Radial-axial Turbines of Small Power" (in Russian), Mashinostroenie, Moscow 1976

[4] Dixon S. L. Fluid Mechanics, Thermodynamics of Turbomachinery, Pergamon Press, Oxford 1975

[5] Kousal. M., "Stationary Gas Turbines" (in Czech), SNTL Prague 1965

[6] Vavra, M. H., Aero-Thermodynamics and Flow in Turbomachines, J. Wiley&Sons, New York 1960

[7] Howell, A. R., The Present Basis of Axial Flow Compressor design: Part 1 – Cascade Theory and Performance, ARC R&M 2095, 1942

[8] Howell, A.R., Fluid Dynamics of Axial Compressors, Proc. I. Mech. E, 153 (1945), #12, pp. 441-452

[9] Dunham, J., Came, P.: Improvements to the Ainley-Mathieson Method of Turbine Performance Prediction. Trans. ASME, Series A, Vol. 92, 1970

[10] Canova M et al., A Scalable Modelling Approach for the Simulation and Design Optimization of Automotive Turbochargers, SAE Technical Paper 2015-01-1288

[11] Vítek O, Macek J and Polášek M, New Approach to Turbocharger Optimization using 1-D Simulation Tools, SAE Paper 2006-01-0438, 2006

[12] Watson N and Janota MS (1982) Turbocharging the Internal Combustion Engine. MacMillan Publishers, London 1982, ISBN 0 333 24290 4

[13] Zinner K., Aufladung von Verbrennungsmotoren, Springer 1975

[14] Shapiro, A. H., The Dynamics and Thermodynamics of Compressible Fluid Flow, The Ronald Press Comp., New York 1953.

[15] Nakhjiri, M., Pelz, P., Matyschok, B., Däubler, L. et al., Physical Modeling of Automotive Turbocharger Compressor: Analytical Approach and Validation, SAE Technical Paper 2011-01-2214, 2011, https://doi.org/10.4271/2011-01-2214.

[16] Bozza, F., De Bellis, V., Marelli, S., and Capobianco, M., 1D Simulation and Experimental Analysis of a Turbocharger Compressor for Automotive Engines under Unsteady Flow Conditions, SAE Int. J. Engines 4(1):1365-1384, 2011, https://doi.org/10.4271/2011-01-1147.

[17] Jerie, J., "Theory of Aircraft Engines" (in Czech), CTU in Prague, 1985

SYMBOLS AND SUBSCRIPTS

A	flow area [m^2]; axial force component [N]
a	sound velocity [m.s^{-1}]; axial Cartesian coordinate; regression coefficient
b	blade length perpendicular to axial or radial direction [m]
c	chord length [m]; specific thermal capacity [J.K^{-1}.kg^{-1}]; absolute velocity [m.s^{-1}]
c_x	drag coefficient [1]
c_y	lift coefficient [1]
h	specific enthalpy [J.kg^{-1}]
K	tuning coefficient [1]
k	tuning coefficient [1; radial shroud clearance [m]
M	Mach number [1]
m	mass, mass flow rate (dotted)[kg, kg.s^{-1}]

n	speed [min^{-1}]
P	power [W]
p	pressure [Pa]; position of maximum distance between airfoil centerline and chord [m]
R	radius [m]
Re	Reynolds number [1]
r	radius [m]; specific gas constant [$J.K^{-1}.kg^{-1}$]
s	cascade step [m]
T	temperature [K]; tangential force component [N]
t	tangential Cartesian coordinate [m]; blade profile thickness [m]
u	circumferential blade speed [$m.s^{-1}$]
w	relative velocity [$m.s^{-1}$]
x	Cartesian coordinate [m]
y	iteration variable
z	number of blades [1]
α	angle of absolute velocity of flow (from radial or axial direction in the sense of speed)[deg]
β	angle of relative velocity of flow (from radial or axial direction) [deg]
β_B	angle of tangent to blade centerline
γ	angle of airfoil chord from axial or radial direction[deg]
δ	flow deviation outlet angle [deg]
ε	flow turn angle [deg]
η	isentropic efficiency [1]
ι	flow incidence angle [deg]
λ	coefficient of secondary losses [1]
φ	polar or cylindrical coordinate angle [deg]
κ	c_p/c_v ratio, isentropic exponent [1]
π	pressure ratio >1 [1]
ρ	density [$kg.m^3$]
σ	angle of oblique shock wave measured from flow velocity direction[deg]
θ	profile centerline turn angle [deg]; flow deviation angle in oblique shock
ζ	loss coefficient [1]
ω	angular velocity [$rad.s^{-1}$]

SUBSCRIPTS

a	axial
B	blade
C	compressor; Cartesian
I	impeller
m	mean
max	maximum
min	minimum
P	polar
p	at constant pressure; profile loss
r	radial
red	reduced
ref	reference
reg	regression
rel	relative state
s	isentropic; flow separation; secondary (induced) loss
sep	flow separation
T	turbine
TC	turbocharger
t	total state; tangential
v	at constant volume
X	drag
Y	lift
0	stagnation state
in	inlet
out	outlet
z	loss
$1, 2, 3..$	position in a compressor
‘	blade root (hub)
“	blade tip (shroud)
*	reference, nominal; critical state of flow
$\bar{}$	averaged
$\vec{}$	vector (if value is used, it has to feature appropriate sign acc. to axis direction)

ACRONYMS

BL	boundary layer
bmep	brake mean effective pressure
CR	centripetal radial
ICE	internal combustion engine
IMEP	indicated mean effective pressure
IRC	internal recirculation channel (anti-surge measure for centrifugal compressors)
MFR	mass flow rate
RPM	revolutions per minute
WOT	wide-open throttle curve